An In Situ Multiscale Study of Ion and Electron Motion in a Lithium-Ion Battery Composite Electrode

ARTICLE *in* ADVANCED ENERGY MATERIALS · AUGUST 2014

Impact Factor: 16.15 · DOI: 10.1002/aenm.201400903

7 AUTHORS, INCLUDING:

J. C. Badot
École nationale supérieure de chimie de Paris
121 PUBLICATIONS **869** CITATIONS
SEE PROFILE

Cristian Perca
11 PUBLICATIONS **102** CITATIONS
SEE PROFILE

Patrick Soudan
Institut des Materiaux Jean Rouxel
38 PUBLICATIONS **605** CITATIONS
SEE PROFILE

Bernard Lestriez
Institut des Materiaux Jean Rouxel
124 PUBLICATIONS **1,525** CITATIONS
SEE PROFILE

An In Situ Multiscale Study of Ion and Electron Motion in a Lithium-Ion Battery Composite Electrode

Kalid-Ahmed Seid, Jean-Claude Badot, Cristian Perca, Olivier Dubrunfaut, Patrick Soudan, Dominique Guyomard, and Bernard Lestriez*

This work reveals the great potential of in situ dielectric spectroscopy for deciphering the motion of ions and electrons on different scales in lithium-ion battery electrodes. One of the main bottlenecks limiting composite electrode kinetics and energy density, is a critical lack of fundamental understanding with respect to the electronic and the ionic transport within the electrode architecture. The latter is a granular material made up of clusters of particles, in which the particles are separated by boundaries that limit the electronic transport. The ionic transport is also severely restricted due to its tortuous porosity. Here, in situ dielectric spectroscopy is used to study the lithium-ion battery $LiNi_{1/3}Co_{1/3}Mn_{1/3}O_2$ composite electrodes. Short- and long-range motions of ions are evident in the low-frequency region. At higher frequencies, the influence of the adsorbed electrolyte ions on the electronic transfer at the micrometer scale is shown.

1. Introduction

For state-of-the-art lithium-ion technology, there is a strong demand for the development of new batteries with improved performance and kWh cost reduction. In order to achieve this goal one needs to design batteries with a higher energy density, which could be achieved by increasing the active mass loading by using thicker and/or denser electrodes.[1–5] However, the electrochemical performance of such electrodes suffers strong kinetic limitations as a consequence of un-optimized electronic transfer and mass transport properties.[6–9] The dc conductivity, σ_{dc}, is the only measured quantity to determine the macroscopic electronic transport, and yields poor information on the electronic transport in composite electrodes. Modelling of polarization-interrupt experiments was recently used to measure effective electrolyte transport in films of porous composite electrodes.[10] The conventional impedance spectroscopy technique (IS) from 10^{-3} to 10^{6} Hz measures several processes in situ, such as macroscopic ionic transport in the electrodes and interfacial charge transfer.[11] Here we use a complementary technique, the broadband dielectric spectroscopy (BDS) technique, to measure complex permittivity of materials over a wide frequency range from few Hz to few GHz, which can detect faster motions, i.e., bulk electrons motion in the MHz-GHz range.[12] The complex conductivity is related to the complex permittivity by

$$\sigma(\omega) = i\omega\varepsilon_0\varepsilon(\omega) = i\omega\varepsilon_0(\varepsilon' - i\varepsilon'') \quad (1)$$

where $\varepsilon_0 \approx 8.84 \times 10^{-12}$ F m^{-1} is the vacuum permittivity and $\omega = 2\pi\nu$ the pulsation expressed in rad s^{-1} (ν being the frequency expressed in Hz). ε' and ε'' are the real and imaginary parts of the permittivity, respectively. Previously,[8,9,13–15] we showed that the dielectric spectra of the conducting materials is expressed by

$$\varepsilon(\omega) = \varepsilon_\infty + \left[\sum_m \frac{\varepsilon_{mL} - \varepsilon_{mH}}{\left(1 + (i\omega\tau_m)^{1-\alpha_m}\right)^{\beta_m}}\right] + A(i\omega)^{s-1} + \frac{\sigma_{dc}}{i\omega\varepsilon_0} \quad (2)$$

where σ_{dc} is the dc-conductivity of the sample, ε_∞ the background permittivity of the compound, τ_m the characteristic time of the relaxation m, s an empirical parameter ($0 \le s \le 1$) and $\Delta\varepsilon_m = (\varepsilon_{mL} - \varepsilon_{mH})$ the dielectric strength of the relaxation m. In Equation (2), the term in brackets is the sum of the susceptibilities of the relaxation mechanisms described by Havriliak-Negami (HN) functions. α_m and β_m are fitting parameters which define the HN-function, which is an empirical modification of the Cole-Cole (CC) function for which $\beta_m = 1$.

In view of the fact that each scale of the material displays a characteristic response (dielectric relaxation) to a given frequency band, it is then possible to determine the multiscale electric polarization mechanisms (bulk, grain boundaries, particles, clusters of particles, sample) (**Figure 1**a) and thus the multiscale conductivities in materials. Up until now, BDS

Dr. K.-A. Seid, Dr. C. Perca, Dr. O. Dubrunfaut
Laboratoire de Génie Electrique de Paris
CNRS, SUPELEC
Sorbonne Universités-UPMC Univ.
Paris 06, Univ. Paris-Sud, 11 rue Joliot-Curie
Plateau de Moulon, 91192, Gif-sur-Yvette, France
Dr. K.-A. Seid, Dr. J.-C. Badot
Institut de Recherche de Chimie Paris
CNRS, Réseau sur le Stockage Electrochimique de l'Energie (RS2E)
CNRS, Chimie ParisTech
11 rue Pierre et Marie Curie, 75005, Paris, France
E-mail: jc.badot@chimie-paristech.fr
Dr. P. Soudan, Dr. D. Guyomard, Prof. B. Lestriez
Institut des Matériaux Jean Rouxel
Réseau sur le Stockage Electrochimique de l'Energie (RS2E)
CNRS, Université de Nantes
44000, Nantes, France

DOI: 10.1002/aenm.201400903

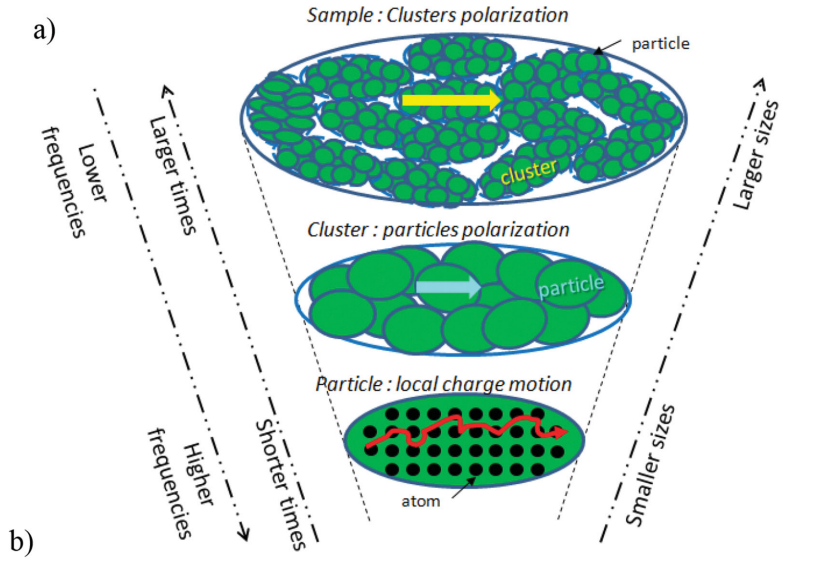

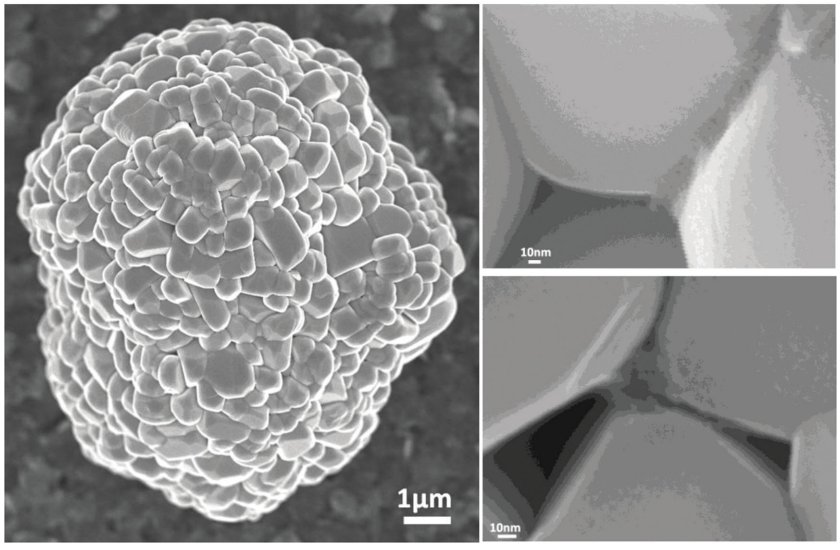

Figure 1. Hierarchical structure of $Li_{1/3}Ni_{1/3}Mn_{1/3}Co_{1/3}O_2$ active material used in composite electrode for lithium batteries. a) SEM images (left) of a quasi-spherical cluster of $Li_{1/3}Ni_{1/3}Mn_{1/3}Co_{1/3}O_2$, and (right) of particles within a cluster. b) Schematic description of the hierarchical architecture within the samples.

characterizations were ex situ measurements and provided a fundamental insight into the multiscale electronic transport in active materials (LiV_3O_8,[13,14] coated $LiFePO_4$[8,9] and $LiNi_{1/3}Ni_{1/3}Co_{1/3}O_2$[15] before being integrated into batteries. However, this property is likely to evolve when the electrode comes in contact with the electrolyte during and after the charge and discharge processes. To study this evolution, we developed a new in situ device in order to take dielectric spectroscopy measurements from 10^3 to 5×10^9 Hz (hereafter called in situ radiofrequency broadband dielectric spectroscopy, i.e., in situ RF-BDS) during electrochemical cycling (**Figure 2**a).

This new device thus provides important new prospects with respect to determining the evolution of multiscale electrical properties (electronic and ionic) during electrochemical cycling.

Hereafter, we propose a completely novel insight into the material/electrolyte interface by way of an NMC-based ($LiNi_{1/3}Ni_{1/3}Co_{1/3}O_2$) composite electrode in a lithium battery using the new device (Figure 2a). In order to understand the charge transport mechanisms, only in situ measurements were performed on the i) dry $LiNi_{1/3}Ni_{1/3}Co_{1/3}O_2$ powder with a 10 µm mean cluster size including particles from 0.4 to 1.3 µm in size (Figure 1b), the ii) dry composite electrode (91.2% $LiNi_{1/3}Mn_{1/3}Co_{1/3}O_2$, 7% PVdF, 1.8% carbon black), and the composite electrode soaked in the electrolyte LP30 (0.1 M of $LiPF_6$ in EC:DMC 1:1), iii) before and iv) after the first charge (incomplete charge up to $Li_{0.6}Ni_{1/3}Ni_{1/3}Co_{1/3}O_2$). Furthermore, complementary ex situ measurements are reported for carbon-coated C-$LiFePO_4$ as Supporting Information (Section 4).

2. Electron Transfer in Dry Electrodes

The real parts of permittivity and conductivity of the different compounds with respect to the frequency were detailed (**Figure 3**a,b). In the dry electrode, the addition of 2% carbon black (CB) drastically increases dc-conductivity by almost three orders of magnitude compared to the NMC powder pellet (Figure 3a). The conductivity of the dry electrode is constant and equal to the dc one up to 10^6 Hz. Above 10^6 Hz, the conductivity is an increasing function of the frequency and is still higher, by about half an order of magnitude, than that of NMC powder, thereby showing that the conductivity is mainly due to the CB. The latter therefore acts as a short-circuit with respect to NMC in the whole frequency range.[13] The real part of the permittivity of the dry electrode (Figure 3b) is higher by almost three orders of magnitude than that of the NMC. Below 10^4 Hz, dry electrode (real) permittivity is a decreasing function of the frequency, since it varies as $\omega^{-1.88}$.

Since all the polarizations at different scales are additive owing to their vectorial character, their contributions (relaxations) can thus be evidenced by a decomposition procedure of the Nyquist plots (imaginary part ε'' vs. real part ε' of permittivity) (**Figure 4**a–c). The power-law frequency-dependent permittivity (ω^{-1}), represented by a quasi-straight line C1 (Figure 4a), corresponds (Equation (2)) to the dc-conductivity contribution of the dry electrode. By subtracting the C1 contribution, two relaxations, C2 (circular arc, Figure 4b) and C3 (skewed arc, Figure 4c) are found with relaxation frequencies of 2×10^7 and 6.6×10^8 Hz, respectively.

These two relaxation frequencies are temperature-independent owing to the quasi-metallic behaviour of CB.[13] The C2 relaxation results in the formation of a space-charge polarization due to the gold-sample interface.[8] The C3 relaxation is described by a HN-

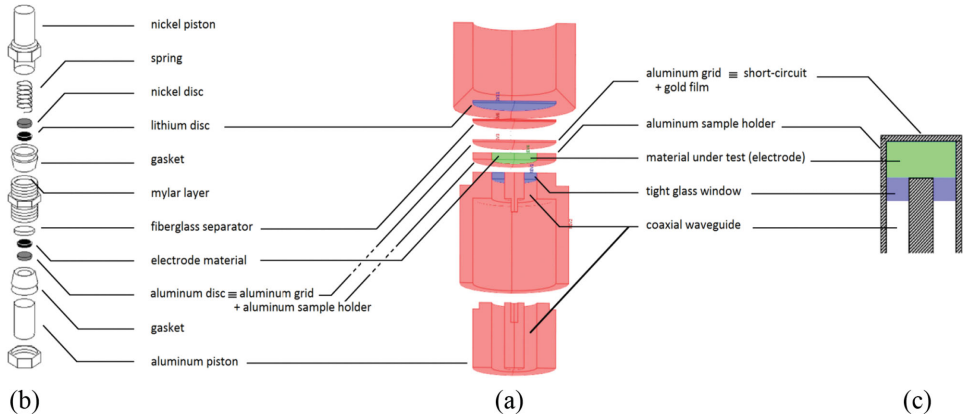

Figure 2. a) Detailed scheme of the in situ device, which is a combination of b) an electrochemical Swagelok cell and c) a coaxial electromagnetic cell.

function, with $\alpha_2 = 0.36$ and $\beta_2 = 0.27$, and can be attributed to the polarization of CB clusters. Non-Debye frequency responses such as these are often observed in random composites very near the percolation threshold, in agreement with the CB clusters being disordered stacks of CB particles. It is to be noted that the relaxation due to CB particles must occur well above the frequency range of NMC electrodes.[13] The relaxations related to the active material (NMC) are not observed because the electron flux goes mainly through the CB network, even though the latter is only slightly above the percolation threshold. Nevertheless, we studied the NMC powder separately.[9] As the frequency increases, various polarizations appear ranging from interatomic

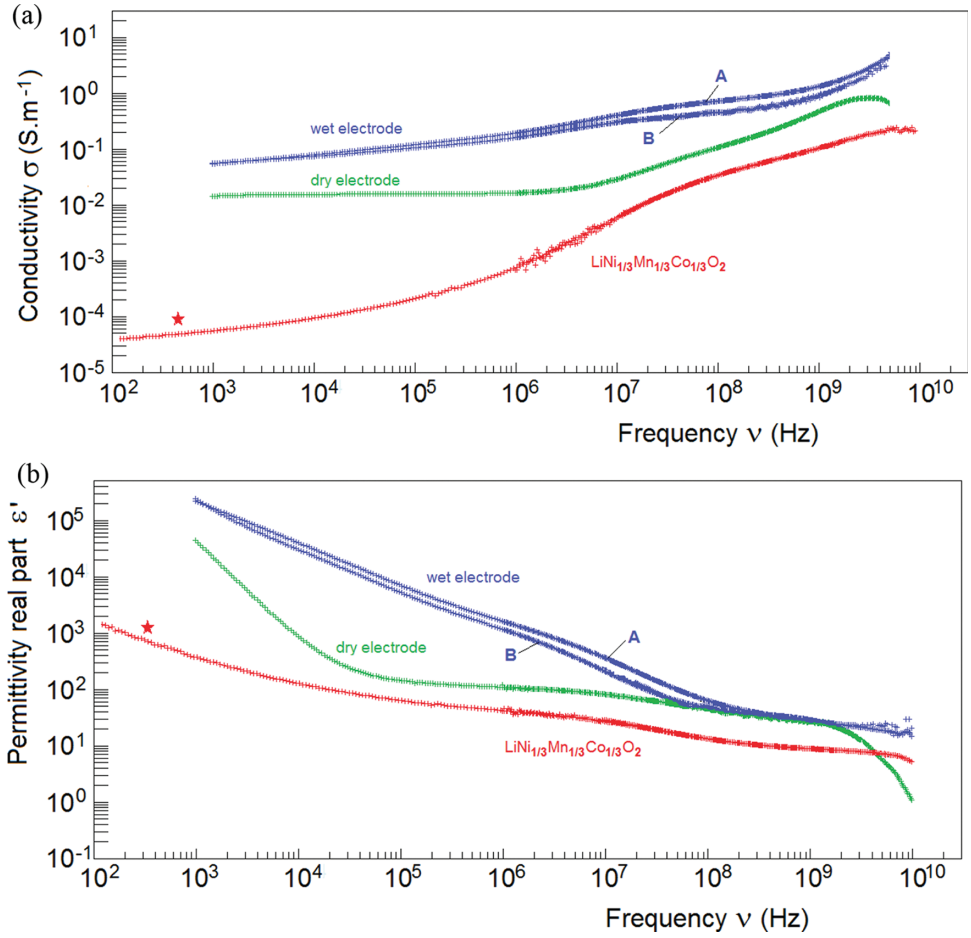

Figure 3. Real parts of the a) conductivity and b) permittivity as function of the frequency for $Li_{1/3}Ni_{1/3}Mn_{1/3}Co_{1/3}O_2$ sample (ex situ measurement, red), dry electrode (in situ measurement, green), and wet electrode (in situ measurement, blue) before (B) and after (A) the 1st charge. ★: ex situ measurement.

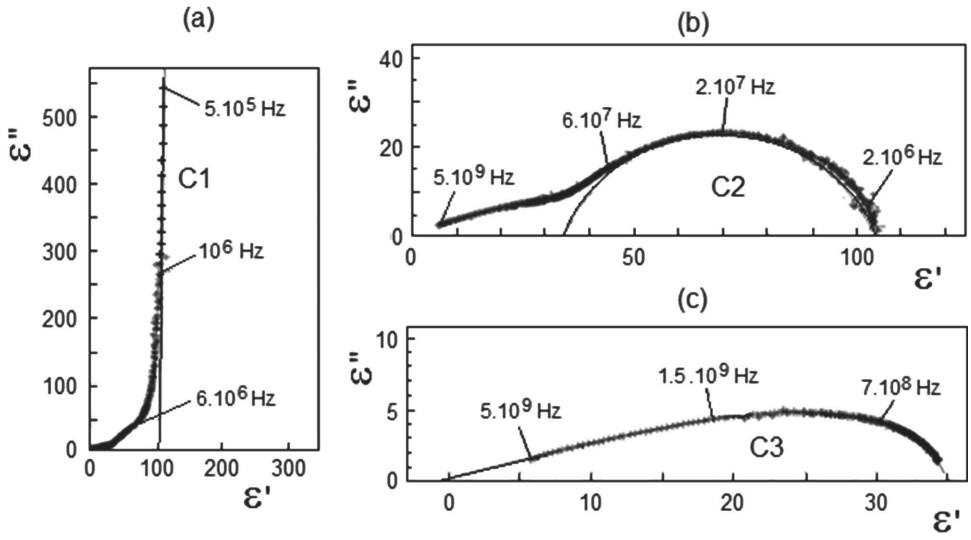

Figure 4. Nyquist plots of the imaginary part $\varepsilon''(\omega)$ vs. the real part $\varepsilon'(\omega)$ of complex permittivity for the dry electrode (91.2 wt% $LiNi_{1/3}Mn_{1/3}Co_{1/3}O_2$, 7% of PVdF, 1.8 wt% of carbon black C-NERGY Super C45) at 300 K. a) Entire plot: only the contribution C1 is visible; b) plot obtained upon subtracting the domain C1: evidence of the relaxation domain C2; and c) plot obtained upon subtracting the domain C2: evidence of the relaxation domain C3.

distances to macroscopic sizes, and give rise to dielectric relaxations in the following order: a) macroscopic space-charge polarization (low-frequency range) due to the sample/current collector interface; b) polarization of clusters of particles (micrometer scale); c) polarization of particles due to the existence of resistive boundary junctions; and d) electron transfers (nanometric or interatomic scale). High interatomic level conductivity was evidenced. However, a large conductivity drop of 3 to 4 orders of magnitude was observed from the particle to the cluster scale, as a consequence of the presence of amorphous grain boundaries between the particles within the clusters. The conductivity drop from the cluster to the sample scale is comparatively very small, owing to the dense architecture of the NMC sample in which the spherical clusters are tightly stacked.

3. Ion Long Range Motions in a Wet Electrode

The addition of the electrolyte enhances the conductivity in the whole frequency range, especially near to 10^7 Hz (Figure 3a) due to its high ionic conductivity (i.e., $\sigma_{electrolyte} \approx 1$ S m^{-1} at RT) and because it fills the pores within the electrode. The relation between dc-conductivities of dry (σ_{de}) and wet (σ_{we}) electrodes can be determined from the modified Archie's law:[16,17]

$$\sigma_{we} = \sigma_{de}(1-\phi)^p + \sigma_{electrolyte}\phi^m \quad (3)$$

where $p = \log(1-\phi^m)/\log(1-\phi)$ and φ is the porosity of the electrode filled with the electrolyte. The two exponents, m and p, depend upon the topology of the two conducting phases (conducting solid matrix and conducting liquid in the pores network) and are thus related to their respective tortuosity. The Equation (3) leads to $m = 2.50$ and $p = 0.12$ from $\sigma_{we} = 0.06$ S m^{-1} (here at 1 kHz and at 300 K), $\sigma_{de} = 0.02$ S m^{-1} (at 300 K), and $\sigma_{electrolyte} = 1$ S m^{-1} (at 300 K) and $\varphi = 0.27$. The exponent m value agrees fairly well with that obtained from electrochemical studies, i.e., 1.50 to 3.8.[6,7,10] We also found that the ionic conductivity is thermally activated with activation energy of about 0.16 eV, which is similar to that of the free electrolyte (Supporting Information Section 2 and Figure S2).[18]

The shape of the real permittivity spectra is completely different when the electrode contains the electrolyte. This suggests that the presence of the electrolyte hides the CB contributions to the electrical polarization throughout the entire frequency range. The existence of the kinks between 10^6 and 10^7 Hz (Figure 3a,b) is due to the appearance of intense dielectric relaxations, one of which is shifted towards a higher frequency by about half an order of magnitude after the first charge (A in Figure 3a). The decomposition of the dielectric spectra for the electrode soaked in the electrolyte (before and after 1st charge), resulted in four contributions (i.e., four dielectric relaxations) (**Figure 5**a–d). Indeed, the two contributions (relaxations) of the carbon black network are not observed (**Table 1**).

They are concealed as the network formed by the liquid electrolyte bypasses the CB network due to the low content of the latter. The four contributions can thus be attributed to charge and/or dipolar motions within the NMC and the electrolyte.

4. Electron Transfer at the Semiconductor-Electrolyte Junction

The mid-frequency relaxation, W3, lies in the same frequency range and has a similar frequency prefactor (i.e., around 3×10^{11} Hz) to that of the NMC cluster polarization, D3 (Table 1). The relaxation frequency of W3 follows an Arrhenius law with an activation energy of $E_3 = 0.29$ eV (**Figure 6**a). This type of polarization, which is due to the accumulation of charges (holes) at cluster boundaries, is made possible because of the existence of small PVdF gaps between them, and because of the porosity. Its response is equivalent to a space-charge relaxation at the cluster size (micrometer range).

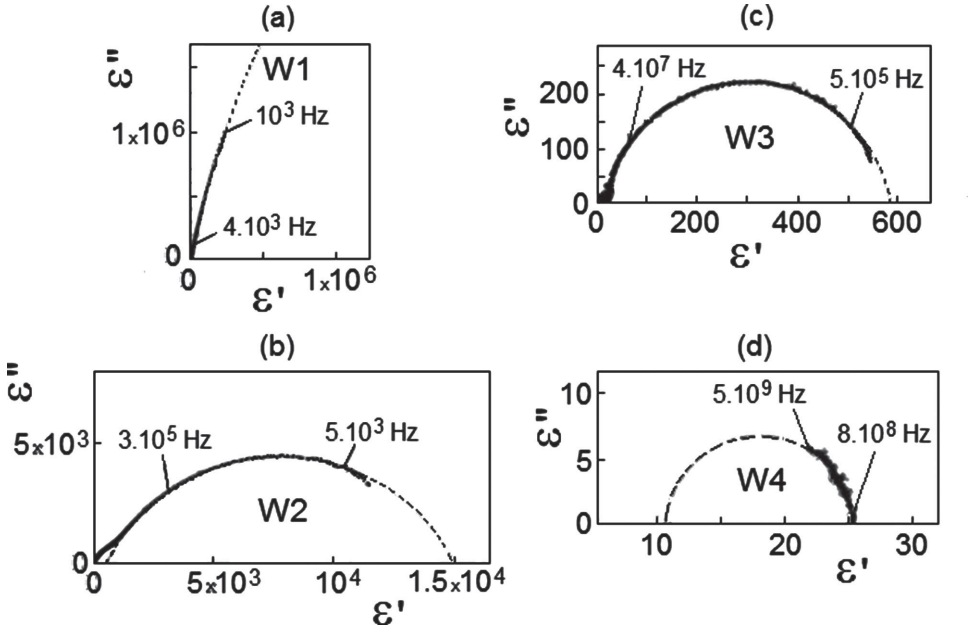

Figure 5. Nyquist plots of the imaginary part $\varepsilon''(\omega)$ vs. the real part $\varepsilon'(\omega)$ of complex permittivity for wet electrodes (91.2 wt% $LiNi_{1/3}Mn_{1/3}Co_{1/3}O_2$, 7% of PVdF, 1.8 wt% of carbon black C-NERGY Super C45) before the charge at 300 K. a) Entire plot: only the contribution W1 is visible; b) plot obtained upon subtracting the domain W1: evidence of the relaxation domain W2; c) plot obtained upon subtracting the domain W2: evidence of the relaxation domain W3; and d) plot obtained upon subtracting the domain W3: evidence of the relaxation domain W4. Electrolyte: LP30 (0.1 M of $LiPF_6$ in EC:DMC 1:1).

As per Figure 6b and Table 1, it is shown that the dielectric strength, $\Delta\varepsilon_3$, of cluster polarization is significantly higher in the presence of the electrolyte: $\Delta\varepsilon_3$ increases from 26 for NMC powder to 571 and 541 before and after the 1st charge, respectively. In order to explain the sharp rise of $\Delta\varepsilon_3$, we need to understand which physical phenomenon occurs at the junction between the semiconductor electrode (NMC) and the electrolyte. For this type of junction, two interfacial regions are created: the first one is comprised of ions adsorbed at the semiconductor surface, and the second one is a space-charge layer of the opposite sign within the semiconductor, in order to equilibrate the two phases electrically. Hence, the sharp rise of the permittivity strength, $\Delta\varepsilon_3$, is caused by the existence of the space-charge region within the NMC cluster in contact with LP30 electrolyte. The relaxation, W3, therefore corresponds to a space-charge relaxation resulting from hole motions through the NMC clusters. For a p-type semiconductor (e.g., NMC), the space-charge region is referred to as a depletion layer (negatively charged) or an accumulation layer (positively charged).[19–21] Moreover, we must determine which type of ion (Li^+ or PF_6^-) is adsorbed at the NMC cluster (or particle) surface, in other words, we need to determine the sign of the space-charge. It is evident that $\Delta\varepsilon_3$ is proportional to the space-charge capacity. Figure 6c shows that $\Delta\varepsilon_3$ increases as the temperature decreases for the wet electrode (before and after the 1st charge). This trend is fitted by an Arrhenius law with an activation energy of E_{sc} = 0.10 eV, before and after the 1st charge. From a theoretical point of view, this behavior is only consistent with the formation of an accumulation layer (Supporting Information Section 3), for which the capacitance, C_{sc}, is given by the approximate Equation:[22]

$$C_{SC} \approx A \exp\left(\frac{V_{SC}}{2kT}\right) \quad (4)$$

where $V_{sc} = 2E_{sc}$ is the energy barrier height corresponding to the built-in voltage involved in the bending of the valence-band (Supporting Information Section 3 and Figure S4). The validity condition $E_{sc} > 3kT$ of Equation (4) is expected. The value of V_{sc} is higher than the difference between the Fermi level and the top of the valence band[9] in the pure NMC, i.e., $|E_{vb}–E_F| \approx$ 0.11 eV (Supporting Information Figure S4). The space-charge is therefore positively charged due to the significant accumulation of holes at the surface of NMC. Hence, this positive charge is compensated by the negative ions PF_6^- of LP30 adsorbed on the NMC surface. Furthermore, the appearance of NMC cluster polarization for the electrode (Figure 5c) occurs with a higher activation energy, E_3 = 0.29 eV, instead of 0.25 eV for the NMC powder[9] (Table 1, Figure 6a). This supplementary barrier, 0.04 eV, is probably due to the existence (in the accumulation layer) of a local electric field that is opposed to the transfer of holes in the NMC lattice at the surface of the clusters.

5. Fast Solvent Motions in the Electrolyte

The faster relaxation, W4, is completely different from those attributed to CB and to NMC, owing to its higher frequency prefactor situated in the infrared range (i.e., around 1.2×10^{13} Hz, Table 1). The relaxation frequency of W4 ($\nu_4 = 10^{10}$ Hz at RT) lies in the range of the relaxation frequencies of the solvent polar molecules, EC and DMC,[23,24] with a mean activation energy of 0.18 eV (Figure 6a). The attribution of this relaxation

Table 1. Relaxation frequency at room temperature, activation energy, frequency prefactor and dielectric strength for different types of motions in $LiNi_{1/3}Mn_{1/3}Co_{1/3}O_2$ (NMC) powder, dry electrode and wet electrode (before and after the 1st charge).

	NMC[a)]	Dry electrode	Wet electrode	
			Before 1st charge	*After 1st charge*
	Frequency (Hz)	Frequency (Hz)	Frequency (Hz)	
	Activation energy (eV)	Activation energy (eV)	Activation energy (eV)	
	Frequency prefactor (Hz)	Frequency prefactor (Hz)	Frequency prefactor (Hz)	
	Dielectric strength Δε	*Dielectric strength Δε*	*Dielectric strength Δε*	
Anion motions in double-layer of electrolyte/NMC cluster interface *(W2)*			2.0×10^4	3.0×10^4
			0.15	0.15
			7×10^6	1×10^7
			1.5×10^4	*1.1×10^4*
NMC cluster polarization *(D3, W3)*	2.0×10^7		3.0×10^6	5.0×10^6
	0.25		0.29	0.29
	4.0×10^{11}		3.0×10^{11}	3.0×10^{11}
	26		*571*	*541*
NMC particle polarization *(D4)*	3.0×10^9			
	0.11			
	3.0×10^{11}			
	2.4			
Solvent dipolar relaxation *(W4)*			1.0×10^{10}	1.0×10^{10}
			0.18	0.18
			1.2×10^{13}	1.2×10^{13}
			14	*18*
CB particle polarization *(C3)*		6.6×10^8		
		0.00		
		6.6×10^8		
		35		

[a)] Ex situ measurements.[9]

is clearly confirmed when using the same solvent to soak a pellet of carbon-coated $LiFePO_4$ (Supporting Information Section 4). The small contribution of NMC particles observed on the dry powder in the GHz range does not appear because the clusters are practically non-porous, and only a small fraction of particles at the cluster surface are in contact with the electrolyte.

6. Ion Transfer at the Semiconductor-Electrolyte Junction

The two low-frequency contributions, W1 and W2, can be attributed to the ions (Li^+, PF_6^-) of the electrolyte. In the lower frequency range, an intense dielectric relaxation (W1) is due to the presence of an ionic double-layer at the sample-electrolyte interface. The relaxation frequency of this double-layer is $\nu_1 = 42$ Hz at room temperature with an activation energy $E_1 = 0.17$ eV (Supporting Information Figure S7), which is very close to the activation energy of the ionic conductivity of the electrolyte. This is meaningful since the product, $\sigma_1 = 2\pi\varepsilon_0\Delta\varepsilon_1\nu_{w1,}$ is homogeneous to a conductivity equal to 4×10^{-2} S m^{-1}, which is of the same order of magnitude as $\sigma_{we} = 6 \times 10^{-2}$ S m^{-1} at 298 K. The W1 relaxation strength $\Delta\varepsilon_1 = (\varepsilon_1 - \varepsilon_s) = 1.76 \times 10^7$ is not dependent on the temperature (**Figure 7**a). ε_1 is the permittivity of the whole sample/double-layer and $\varepsilon_s = 600$ is the sample permittivity.

Since $\varepsilon_s << \varepsilon_1$, it follows that $\Delta\varepsilon_1 \approx \varepsilon_1$ and the double-layer capacitance C_{dl} is given by:

$$C_{dl} = \varepsilon_0\varepsilon_1\frac{S}{L_S} = \varepsilon_0\varepsilon_{solv}\frac{S}{L_D} \quad (5)$$

with $L_D = L_S(\varepsilon_{solv}/\varepsilon_1)$. $S = \pi r^2$ is the sample area (with $r = 3.5$ mm, the sample radius), L_s the sample thickness, L_D the Debye length (i.e., ionic double-layer thickness), and ε_{solv} the permittivity of the solvent, EC:DMC (1:1). From the Equation (5), the double-layer capacitance is $C_{dl} = 40$ µF cm^{-2}, which lies within the range of the values generally found. The permittivity of a mixed solvent such as EC:DMC can be given by:[25]

$$\varepsilon_{solv} = \phi_{DMC}\varepsilon_{DMC} + \phi_{EC}\varepsilon_{EC} \quad (6)$$

where ε_{DMC}, ε_{EC} are the permittivities, and φ_{DMC}, φ_{EC} the volume fractions of DMC and EC, respectively. The Equation

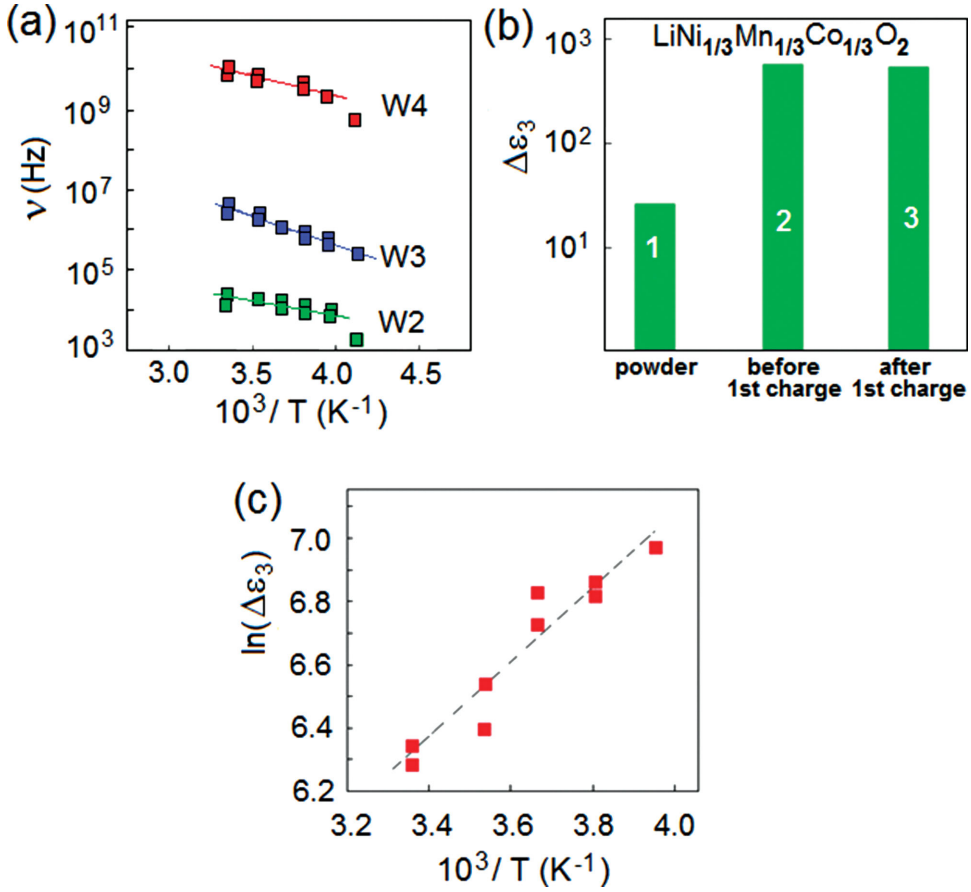

Figure 6. Dielectric relaxation frequencies observed for composite electrodes. a) Relaxation frequencies ν_{w2}, ν_{w3} and ν_{w4} of the relaxations W2, W3 and W4 as function of inverse temperature T^{-1} in wet electrode (before and after the charge). b) Dielectric strength $\Delta\varepsilon_3$ of the relaxation W3 due to cluster polarization as function of the sample configurations (1: $Li_{1/3}Ni_{1/3}Mn_{1/3}Co_{1/3}O_2$ powder; 2: wet electrode before the 1st charge; 3: wet electrode after the 1st charge). c) Dielectric strength $\Delta\varepsilon_3$ of the relaxation W3 as function of inverse temperature T^{-1} (log $\Delta\varepsilon_3$ vs. T^{-1}) in wet electrode. Electrode: 91.2 wt% $LiNi_{1/3}Mn_{1/3}Co_{1/3}O_2$, 7% of PVdF, 1.8 wt% of carbon black C-NERGY Super C45) and electrolyte: LP30 (0.1 M of $LiPF_6$ in EC:DMC 1:1).

(6) yields $\varepsilon_{solv} = 39.5$ with $\varepsilon_{DMC} = 3.11$, $\varepsilon_{EC} = 89.7$, $\varphi_{DMC} = 0.58$ and $\varphi_{EC} = 0.42$. Since the sample thickness is $L_S = 0.38$ mm, the Equation (5) gives $L_D = 0.85$ nm, which is in the order of magnitude of a double-layer thickness.

The relaxation, W2, is due to a polarization associated with the ion motions in the electrolyte-filled pores. This is confirmed by the gradual disappearance of its dielectric strength, $\Delta\varepsilon_2$ ($\Delta\varepsilon_2 \rightarrow 0$), by freezing the electrolyte below 243 K (Figure 7b).

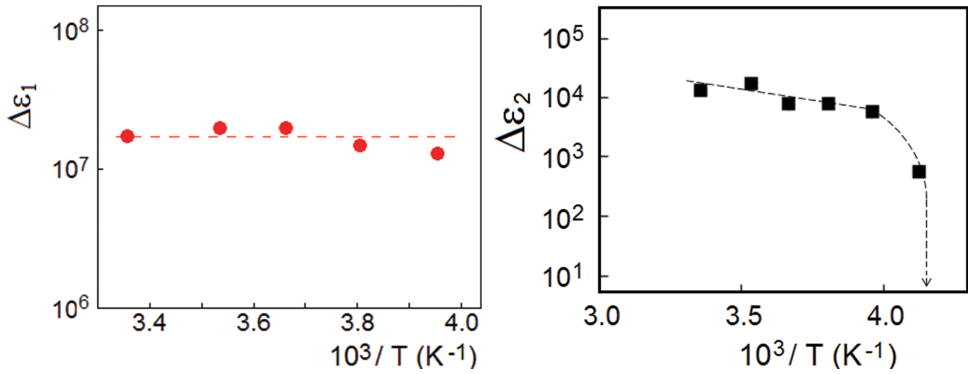

Figure 7. a) Dielectric strength $\Delta\varepsilon_1$ (proportional to the double-layer capacitance) of the relaxation W1 attributed to the ionic double-layer relaxation at the electrode surface ((91.2% $LiNi_{1/3}Mn_{1/3}Co_{1/3}O_2$, 7% PVdF, 1.8% carbon black). b) Dielectric strength $\Delta\varepsilon_2$ of the relaxation W2 as function of inverse temperature T^{-1} (log $\Delta\varepsilon_2$ vs. T^{-1}) in wet electrode. Electrode: 91.2 wt% $LiNi_{1/3}Mn_{1/3}Co_{1/3}O_2$, 7% of PVdF, 1.8 wt% of carbon black C-NERGY Super C45) and electrolyte: LP30 (0.1 M of $LiPF_6$ in EC:DMC 1:1).

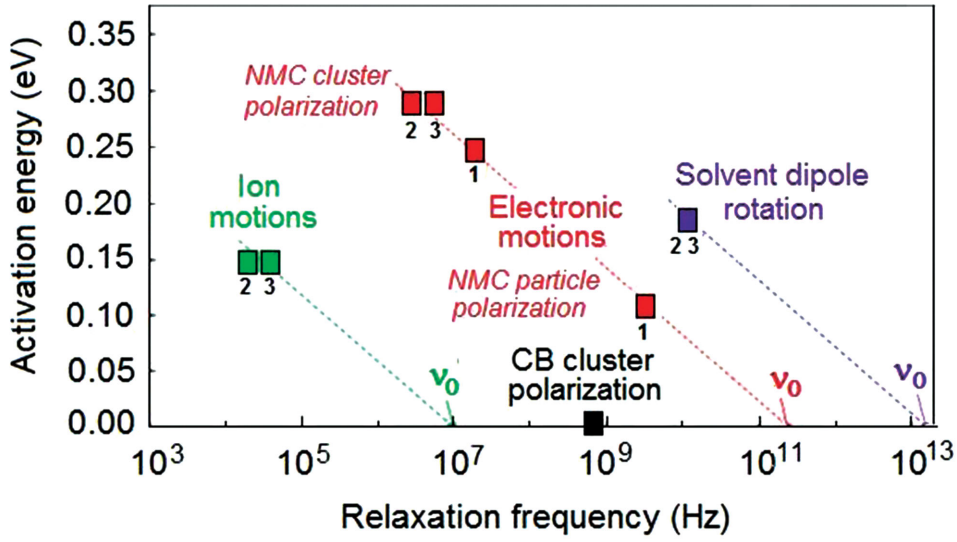

Figure 8. Activation energies vs. relaxation frequencies (at 298 K) attributed to the different types of motions: PF_6^- diffusion in pores filled with electrolyte, $Li_{1/3}Ni_{1/3}Mn_{1/3}Co_{1/3}O_2$ (NMC) clusters and particle polarizations due to hole motions, electron motions in carbon black (CB) and solvent molecule rotations. The slope of the dotted line corresponds to the thermal energy at 298 K and yields the mean frequency prefactor (at zero energy) of the hole motions in NMC. (1: $Li_{1/3}Ni_{1/3}Mn_{1/3}Co_{1/3}O_2$ powder; 2: wet electrode before the 1st charge; 3: wet electrode after the 1st charge).

Before and after the first charge, W2 has a mean characteristic frequency of $\nu_2 = 2.5 \times 10^4$ Hz (at 300 K), which is thermally activated with an activation energy of $E_2 = 0.15$ eV (Table 1, Figure 6a) that is similar to the electrolyte dc-conductivity one ($E_{electrolyte} = 0.16$ eV). The relaxation, W2, can thus be attributed to PF_6^- motions, since they are preferentially adsorbed on the NMC clusters surface. These motions are short-range hopping between the adsorption sites, especially at the surface of crystallized particles belonging to the clusters (Supporting Information Section 4). This means the relaxation W2 occurs within the local ionic double-layer at the NMC cluster-electrolyte interface along which the ionic (i.e. PF_6^- counter-ions) motions take place. The relaxation W2 is therefore due to the double-layer polarization parallel to the cluster surface. Furthermore, a correlation exists between the electrolyte dc-conductivity, σ_{we}, and the dielectric relaxation strength, $\Delta\varepsilon_2$. The product $\sigma_{\Delta\varepsilon} = 2\pi\varepsilon_0\Delta\varepsilon_2\nu_{w2}$ is homogeneous to a conductivity equal to 2×10^{-2} S m^{-1} of the same order of magnitude as $\sigma_{we} = 6 \times 10^{-2}$ S m^{-1} at 298 K. This correlation between the dc-conductivity and the dielectric relaxation strength, which has been found for many conducting materials, is further evidence of the assignment of W2 to ion short-range motion in the pore-filled electrolyte. We can consider that the products σ_1 and σ_2 are proportional to ion diffusion coefficients D_1 (i.e., on the scale of the sample) and D_2 (i.e., on the scale of the cluster) respectively. By using this assumption, the products $D_1\tau_{w1}$ and $D_2\tau_{w2}$ (with $\tau_{w1} = 1/\omega_{w1}$ and $\tau_{w2} = 1/\omega_{w2}$) are proportional to the squares of the mean diffusion lengths x_1^2 and x_2^2 respectively. As $\Delta\varepsilon_1 \propto x_1^2$ and $\Delta\varepsilon_2 \propto x_2^2$, the ratio $(x_1/x_2) \propto (\Delta\varepsilon_1/\Delta\varepsilon_2)^{1/2}$ is approximately equal to 37 by taking the mean values $\Delta\varepsilon_1 = 1.78 \times 10^7$ and $\Delta\varepsilon_2 = 1.3 \times 10^4$. This ratio agrees with the ratio (sample thickness 380 µm)/(cluster diameter 10 µm) = 38. In this way, $\Delta\varepsilon_2$ corresponds to a local double-layer capacitance which is very large compared to $\Delta\varepsilon_3$, as frequently observed in several systems. The verity of ionic adsorption on the NMC surface is substantiated by the fact that the ionic residence time, τ_{res}, should be shorter than the ionic short-range diffusion time, $\tau_{w2} = 6$ µs (at 298 K), but longer than the cluster relaxation time, $\tau_{w3} = 40$ ns (at 298 K), to induce a space-charge layer inside the active material.

7. Conclusion

The plot of the activation energy as a function of the relaxation frequency (at 300 K) shows that the different types of polarizations are well-discriminated and scheduled, due to the knowledge of the activation energies and the prefactors of their characteristic frequencies (**Figure 8**). All the electronic contributions (CB, NMC clusters and particles) occur at high frequencies (i.e., above 10^6 Hz), while the ionic contributions lie at lower frequencies (i.e., below 10^5 Hz). These results show that in situ RF-BDS does indeed provide additional information when compared to the results of conventional low-frequency impedance spectroscopy.

For instance, for frequencies above 10^7 Hz, the conductivity after 1st charge is twice as large as that before the 1st charge. In this frequency range, which is higher than the characteristic frequency of the clusters, the conductivity corresponds to the intrinsic conductivity of NMC. The increase in conductivity is due to the increase in the number of holes corresponding to the decrease of Li^+ content in the NMC, as observed in a previous paper.[26] The local electric field that exists within the space-charge layer of the NMC surface is directed towards the electrolyte and could thus aid in the extraction of lithium-ion from the NMC. Complementary measurements for C-$LiFePO_4$, which are detailed in Supporting Information Section 4, show and confirm the influence of ions and polar molecules on the electrical properties of the active materials.

In summary, this study is the first to demonstrate the influence of the ions in the electrolyte on the transfer of the electronic charges in composite electrodes at the micronic scale,

thus proffering key information about this little-understood interface between the electrolyte and the semiconductor active material. The results also give access to the tortuosity of the electrode, which is a critical aspect when considering the power performance of the battery.

8. Experimental Section

New In Situ RF-BDS Cell: The new in situ device (Figure 2a) combined electrochemical and electrical measurements by radio-frequency broadband dielectric spectroscopy (RF-BDS from 10^3 to 5×10^9 Hz) without mutual interference. It was based on two existing cells: the Swagelok cell widely used for electrochemical studies of batteries (Figure 2b)[27] and a classical BDS cell[28] (Figure 2c). In the Swagelok cell, the positive and negative electrodes were in contact with aluminum and nickel plungers, respectively. Both electrodes were separated by a porous glass paper separator soaked in the electrolyte. To ensure valid contacts between the cell components, a stainless steel spring that exerted a pressure of about 10^5 Pa was located between the nickel disk and the second plunger. The applied voltages between both electrodes and the current were measured at the top of the two pistons. The classical BDS cell was suitable for ex situ measurements (from 40 to 10^{10} Hz) of the complex permittivity and conductivity of the sample under test with respect to the frequency. These complex parameters were obtained from the admittance (or from the reflection coefficient) of the cell loaded with the sample. From the electromagnetic point of view, the aluminum plunger (current collector on the side of the positive electrode) was transformed into a coaxial conductor. An air-tight glass window (thickness = 1.8 mm and dielectric constant $\varepsilon' = 6.5$) separated the inner conductor from the outer conductor of the coaxial waveguide. Metallic contacts were made by sputtering gold directly on both faces of the electrode in order to provide good contacts with: a) the inner conductor of the coaxial waveguide and b) the grid. The first one was only deposited in the center of one (thickness = 300 nm) and the second over the entire opposite face with a thickness of about 50 nm to facilitate the access of the electrolyte through it.[29] The grid and the gold deposited between the electrode and the grid acted as an electric wall (i.e., a short-circuit) for the electromagnetic wave. Thus the electromagnetic wave explored only the electrode under testing (here, the positive electrode) and not the battery (e.g., the separator and the counter-electrode). The electromagnetic problem solved for the classical BDS cell was therefore applicable to RF-BDS in situ cell (called RF-BDS owing to the frequency range 10^3 to 5×10^9 Hz). The new cell was validated from an electromagnetic point of view (Supporting Information Figure S1).

Materials: The positive electrode composition was 91.2 wt% $LiNi_{1/3}Mn_{1/3}Co_{1/3}O_2$ (MX10 from Umicore), 7% PVdF, and 1.8 wt% carbon black C-NERGY Super C45 (C45 from TIMCAL, density = 1.86 $g.cm^{-3}$, BET surface area = 45 $m^2.g^{-1}$). The positive electrode was prepared by mixing all its constituents in *N*-methyl-pyrrolidone (NMP) for 24 h. After evaporation of the NMP at 80 °C under vacuum, a cylindrical pellet of 7 mm in diameter was prepared from the powder by densification under a pressure of 500 MPa. This electrode was 0.38 mm thick and contained 40 mg of MX10. The porosity was calculated from its geometrical dimensions and the density of the constituents. After Au sputtering for contacts, the pellet was again dried under vacuum at 50 °C for 1 h, and then transferred under dry argon atmosphere in a glove box (H_2O, 1 ppm) for battery assembly according to Figure 2a: an aluminum grid as the current collector, a porous paper soaked with the electrolyte as the separator, and lithium metal as the negative electrode. The electrolyte used was a 1 M $LiPF_6$ solution in an ethylene carbonate/dimethyl carbonate mixture (EC/DMC 1/1 w/w), (Merck LP30).

Measurements: A battery was assembled within the in situ cell by using the positive composite electrode. Incomplete cell charge (up to $Li_{0.6}Ni_{1/3}Mn_{1/3}Co_{1/3}O_2$ corresponding to a voltage of 4.5 V vs. the Li^+/Li reference) was performed at 20 °C, and monitored by an SP-200 system (BIO-LOGIC) in galvanostatic mode, at a rate of C/200. The voltage between the reference electrode and the counter-electrode and the lithium insertion rate were measured at the same time. Permittivity and conductivity measurements were performed between 10^3 and 5×10^9 Hz with an in situ cell connected by a switch to three impedance and network analyzers: Agilent 4294 (40–1.1×10^8 Hz), 4291 (10^6–1.8×10^9 Hz), and E8364B (10^6–5×10^{10} Hz, used up to 5×10^9 Hz). Beforehand, all systematic errors generated by the analyzers, the switch, the coaxial guides and the dc-block (to isolate the analyzers from the battery) were removed and the reference plane (i.e., face of the tight window on the coaxial waveguide side, Figure 2a) was defined, using a calibration process called the short open load method. The rest time before a dielectric measurement after a cycle was set to 24 h so that the potential reached equilibrium.

Supporting Information

Supporting Information is available from the Wiley Online Library or from the author.

Acknowledgements

Authors from the LGEP, IRCP and IMN laboratories thank the ANR program No. ANR-09-STOCK-E-02–01 and the CNRS for funding, as well as UMICORE for its support. The authors thank N. Stephant for SEM observations.

Received: May 30, 2014
Revised: July 17, 2014
Published online:

[1] W. Porcher, B. Lestriez, S. Jouanneau, D. Guyomard, *J. Electrochem. Soc.* **2009**, *156*, A133.
[2] W. Lu, A. Jansen, D. Dees, P. Nelson, N. R. Veselka, G. Henriksen, *J. Power Sources* **2011**, *196*, 1537.
[3] W. Lai, C. K. Erdonmez, T. F. Marinis, C. K. Bjune, N. J. Dudney, F. Xu, R. Wartena, Y. M. Chiang, *Adv. Mater.* **2010**, *22*, E139.
[4] C. J. Bae, C. K. Erdonmez, J. W. Halloran, Y. M. Chiang, *Adv. Mater.* **2013**, *25*, 1254.
[5] D. Mazouzi, D. Reyter, M. Gauthier, P. Moreau, D. Guyomard, L. Roué, B. Lestriez, *Adv. Energy Mater.* **2014**, 10.1002/aenm.201301718.
[6] C. Fongy, A. C. Gaillot, S. Jouanneau, D. Guyomard, B. Lestriez, *J. Electrochem. Soc.* **2010**, *157*, A885.
[7] D. P. Singh, F. M. Mulder, A. M. Abdelkader, M. Wagemaker, *Adv. Energy Mater.* **2013**, *3*, 572.
[8] K. A. Seid, J. C. Badot, O. Dubrunfaut, S. Levasseur, D. Guyomard, B. Lestriez, *J. Mater. Chem.* **2012**, *22*, 2641.
[9] K. A. Seid, J. C. Badot, O. Dubrunfaut, M. T. Caldes, N. Stephant, L. Gautier, D. Guyomard, B. Lestriez, *Phys. Chem. Chem. Phys.* **2013**, *15*, 19790.
[10] N. A. Zacharias, D. R. Nevers, C. Skelton, K. Knackstedt, D. E. Stephenson, D. R. Wheeler, *J. Electrochem. Soc.* **2013**, *160*, A306.
[11] R. De Levie, in *Advances in Electrochemistry and Electrochemical Engineering*, Vol. *6*, (Ed: P. Delahay), Interscience, New York **1967**, p. 329.
[12] N. Bonanos, B. C. H. Steele, E. P. Butler, in *Impedance Spectroscopy*, (Ed: E. Barsoukov, J. R. MacDonald), Wiley, Hoboken, **2005**, p. 205.
[13] J. C. Badot, E. Ligneel, O. Dubrunfaut, D. Guyomard, B. Lestriez, *Adv. Funct. Mater.* **2009**, *19*, 2749.
[14] J. C. Badot, E. Ligneel, O. Dubrunfaut, J. Gaubicher, D. Guyomard, B. Lestriez, *Phys. Chem. Chem. Phys.* **2012**, *14*, 9500.

[15] K. A. Seid, J. C. Badot, O. Dubrunfaut, S. Levasseur, D. Guyomard, B. Lestriez, *J. Mater. Chem.* **2012**, *22*, 2641.
[16] P. W. J. Glover, *Geophysics* **2010**, *75*, E247.
[17] P. W. J. Glover, M. J. Hole, J. Pous, *J. Earth Planetary Sci. Lett.* **2000**, *180*, 369.
[18] L. Lombardo, S. Brutti, M. A. Navarra, S. Panero, P. Reale, *J. Power Sources* **2013**, *227*, 8.
[19] L. M. Peter, in *Comprehensive Chemical Kinetics*, (Ed: R. G. Compton, G. Hancock), Elsevier, Amsterdam **1993**, p. 223.
[20] R. J. D. Miller, G. McLendon, A. J. Nozik, *Surface Electron-Transfer Processes*, VCH Publishers, New York **1995**.
[21] K. Rajeshwar, *Encyclopedia of Electrochemistry*, Wiley-VCH Verlag GmbH & Co, Weinheim, Germany **2007**.
[22] N. Sato, *Electrochemistry at Metal and Semiconductor Electrodes*, Elsevier, Amsterdam **2003**.
[23] R. Payne, I. E. Theodorou, *J. Phys. Chem.* **1972**, *76*, 2892.
[24] R. Chandra, M. Xu, P. Firman, E. M. Eyring, S. Petrucci, *J. Phys. Chem.* **1993**, *97*, 12127.
[25] K. Xu, *Chem. Rev.* **2004**, *104*, 4303.
[26] X. Y. Qiu, Q. C. Zhuang, Q. Q. Zhang, R. Cao, Y. H. Qiang, P. Z. Ying, S. G. Sun, *J. Electroanal. Chem.* **2012**, *687*, 35.
[27] D. Guyomard, J. M. Tarascon, *J. Electrochem. Soc.* **1992**, *139*, 937.
[28] N. E. Belhadj, A. Fourrier-Lamer, *IEEE Trans. Microwave Theory Tech.* **1986**, *34*, 346.
[29] G. Chen, T. J. Richardson, *J. Power Sources* **2010**, *195*, 5387.